Preprint
UCRL-JC-145173

Update on Optical Design of Adaptive Optics System at Lick Observatory

B. J. Bauman, D. T. Gavel, K. E. Waltjen, G. J. Freeze, R. L. Hurd, E. L. Gates, C. E. Max, S. S. Olivier, D. M. Pennington

This article was submitted to
46th Annual Meeting, The International Sysmposium on Optical Science and Technology, San Diego, CA, July 29 - Aug. 3, 2001

U.S. Department of Energy

Lawrence
Livermore
National
Laboratory

July 31, 2001

Update on optical design of adaptive optics system at Lick Observatory

Brian J. Bauman[a], Donald T. Gavel[a], Kenneth E. Waltjen[a], Gary J. Freeze[a], Randy L. Hurd[a], Elinor L. Gates[b], Claire E. Max[a], Scot S. Olivier[a], Deanna M. Pennington[a]

[a]Lawrence Livermore National Laboratory, L-290, Livermore, CA 94550
[b]University of California Observatories/Lick Observatory

ABSTRACT

In 1999, we presented our plan to upgrade the adaptive optics (AO) system on the Lick Observatory Shane telescope (3m) from a prototype instrument pressed into field service to a facility instrument.[1] This paper updates the progress of that plan and details several important improvements in the alignment and calibration of the AO bench. The paper also includes a discussion of the problems seen in the original design of the tip/tilt (t/t) sensor used in laser guide star mode, and how these problems were corrected with excellent results.

Keywords: Adaptive optics, deformable mirrors, wavefront sensors, Lick Observatory, laser guide star, sodium guide star

1. INTRODUCTION

The laser guide star/adaptive optics system at the Lick Observatory Shane 3m telescope has been in operation since 1994, with the first significant sodium laser guide-star (LGS) correction occurring in 1996.[2,3] The adaptive optics bench and layout in use during 1996-1998 was an engineering prototypical/experimental unit. The LGS/AO system has performed well, setting records for LGS performance.[4,5] In 1999, we implemented a partial redesign and re-layout of the AO bench with the goal of transferring the AO bench day-to-day operation/maintenance to Lick Observatory and obtaining an easy-to-use, reliable, maintainable system with high observing efficiency on the sky. In particular, we needed to improve the optomechanical stability of key components such as the fast wavefront sensor (WFS), reduce noncommon path errors (particularly non-common powered optics), incorporate calibration techniques/instrumentation into easy, fast, and nonintrusive equipment, and implement a wide-field-of-view acquisition scheme to aid capturing NGS and natural t/t stars in LGS mode.

2. SYSTEM DESCRIPTION

The Lick laser guide star/adaptive optics system is installed at the f/17 cassegrain focus of the 3m Shane Telescope. Most of the major components of the system are as given in reference 3 and are summarized in the following table:

Deformable mirror	LLNL-built, 127 actuators, 61 actuators controlled, triangular pattern, electrorestrictive (PMN) actuators
T/t mirror	3" mirror mounted on Physik Instrumente 2-axis tilt platform, 1200Hz bandwidth
Fast wavefront sensor	Shack-Hartmann wavefront sensor, 40 subapertures (44cm diameter on primary), Adaptive Optics Associates camera with Lincoln Lab 64x64 CCD, read noise 7e^- per pixel at 1200 frames/sec; 4x4 center-of-mass or quad-cell centroiding algorithm
Tip-tilt sensor	Quad-cell photon-counting avalanche photodiode with ±2arcsec FOV, pupil imaged onto the fibers feeding APD's
Wavefront control computer	160Mflop Mercury VME with 4 Intel i860 processors, operated at up to 500Hz sample rate, with 0db crossover up to 30Hz.

Laser guide star	Sodium beacon--tunable dye laser, pumped by flash-lamp-pumped frequency doubled Nd:YAG lasers, launched by 30cm aperture refractive telescope, 18 W average power with 100ns pulse width and 11kHz repetition rate.
Infrared camera	PICNIC HgCdTe 256x256 CCD, 30e^- read noise, .02e^- per second dark current, 1.15x relay optics, 0.076 arcsec/pixel.,800-2550nm, 77K, QE>60%, speckle/subarray/coronagraph modes, 14 filters+blank+open (including grisms) [6]; this upgrades the LIRC-II camera described in reference 3.
Visible scoring camera	Photometrics CH250 (1035x1317, 6.8μ pixels, Kodak 0400 detector, thermoelectrically cooled)
Slow wavefront sensor	Similar to fast wavefront sensor, but using Photometrics CH250 CCD described above

3. LAYOUT/DESIGN

The Lick AO bench optical layout design is shown in figures 1 and 2. Light from the telescope enters from top center on figure 1 and hits two turning mirrors, the t/t mirror, an off-axis parabolic collimating mirror, the deformable mirror, then an off-axis parabolic focusing mirror. The light is then split at a dichroic. The light longer than 900nm (and also 1.5% of the light at 532nm, for the phase-shifting diffraction interferometer (PSDI) is transmitted through the 1st dichroic to a pair of turning mirrors that align the beam into the infrared camera. Just before IRCAL, a mirror may be driven into the light path to reflect the light into the phase-diffraction interferometer; this is used to calibrate the wavefront sensor. The light that is reflected off the "1st dichroic" (<900nm) is then sent to a "2nd dichroic" (in LGS mode; in NGS mode, the dichroic is replaced by a 90%R/10%T spectrally-flat beamsplitter-- this is planned to be a remotely-actuated replacement). The light that is <600nm is reflected off the 2nd dichroic to a fold mirror and into the fast wavefront sensor. An iris, nominally located at the focus of the wavefront sensor beam (this will be discussed later) rejects LGS Rayleigh scatter. The iris' diameter and position can be controlled remotely to maximize unwanted light rejection. The rest of the wavefront sensor leg consists of a collimating lens, lenslet array, relay optics, and AOA wavefront sensor camera. The light that is transmitted through the 2nd dichroic (600-900nm in LGS mode; 10% of <900nm in NGS mode) then hits a beamsplitter cube. 10% of that light is transmitted to the scoring/acquisition camera. The remaining 90% of the light is reflected towards the table, where it strikes a second, smaller beamsplitter cube. 90% of that light is reflected into the APD t/t sensor, while the remaining 10% is transmitted through a hole in the table to a slow wavefront sensor on the back side of the table. The purpose of the slow wavefront sensor is to monitor focus and other slowly varying aberrations introduced by the laser guide star. The t/t sensor and the slow wavefront sensor look at the t/t star in LGS mode—in NGS mode, they are ignored.

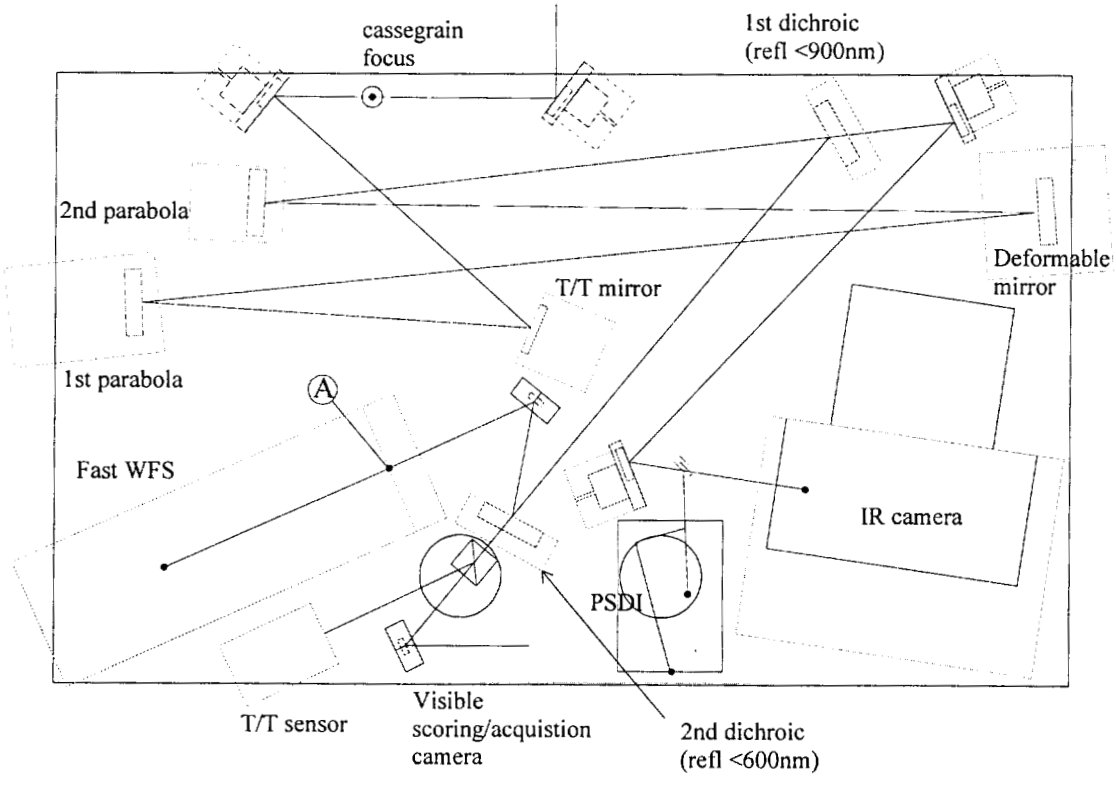

Figure 1: Layout of front side of AO bench. Light enters at the top center of the figure from the telescope. See text for description. Position A is the calibration fiber position described in section 5.

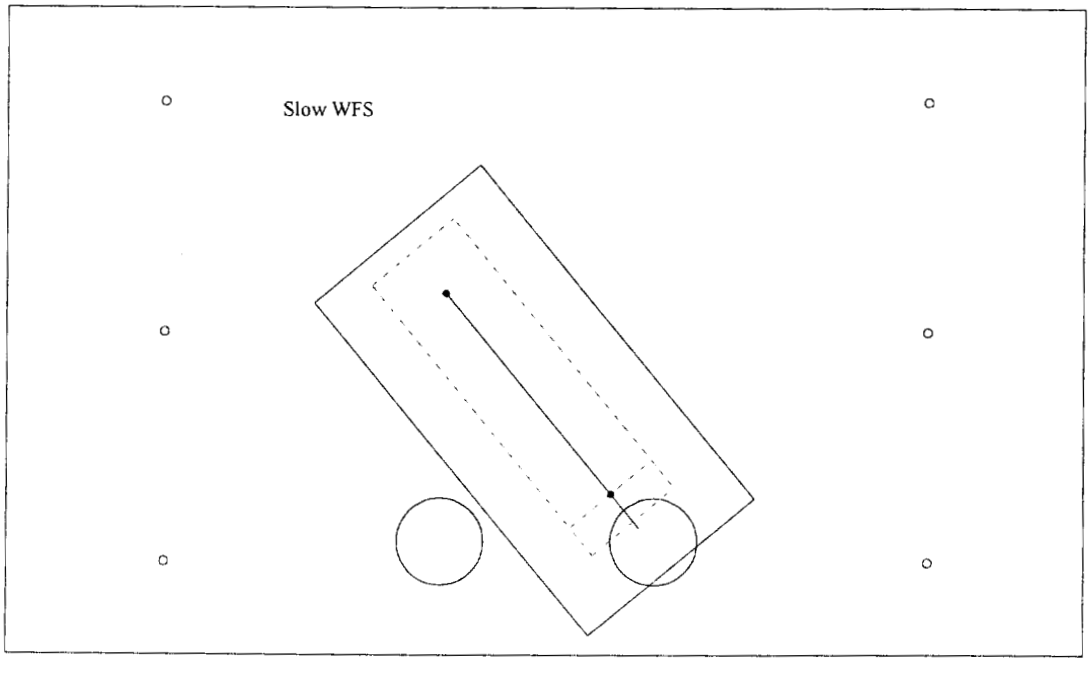

Figure 2: Back side of AO bench. Light comes through hole in table from other side and is folded into slow WFS.

4. STATUS OF PLANNED CHANGES

Table 1 summarizes the list of planned changes from 1999 and their current status.

Feature	Plan	Status
System layout	As shown in figures 1 and 2 and described in reference 1	Implemented; very successful with much more reliable system behavior
Acquisition camera	Flip-in Bravais lens to convert f/17, 20 arcsec field to f/5.8 120 arcsec field	Implemented, but turned out to not be necessary; could use autoguider camera as acquisition camera and boresight to t/t sensor with bright star
Fast wavefront sensor	Use common parabola for both science and WFS legs. Use Newport 462 and 562 stages to produce more stable optomechanics.	Implemented; very successful
PSDI	Set up PSDI to measure aberrations of AO bench[7]	Implemented, but finding Nd:YAG laser with stable wavelength has been problematic. Currently not used, but absence is not limiting performance.
Field-steering control system	Use pairs of mirrors to allow independent steering of science leg, fast WFS leg, and natural t/t star leg	Implemented and integrated into IR camera software/scripts so that camera operator can nod telescope, counter-nod field steering mirrors, and close loop with a single push-button command.

Table 1: Changes planned in 1999 and their current status

5. OTHER CHANGES AND IMPROVEMENTS

1. Tip-tilt sensor

The original design of the t/t sensor is shown below in figures 3 and 4. In this design, light from the f/27 focus is relayed by a lens to an f/250 focus. At this focus, the light strikes a quad lens. The quad lens is formed by cutting four lenses and gluing them together so that their optical axes are about each 4.35mm away from the center of the quad lens (figure 5). The quad lens divides the incident light into 4 quadrants similar to a quad cell. Each lens of the quad lens images the pupil of the system onto a separate multimode 100 micron fiber which feeds separate avalanche photo diodes (APD's). As the image moves around on the sky and the t/t sensor, the relative amounts of light to the APD's change. Closing the loop controls the t/t mirror to center the spot on the quad lens. The t/t mirror's quasi-static displacements are offloaded to the telescope pointing controller so that the t/t mirror does not run out of range.

A long-standing problem in using the t/t sensor has been that the total light collected by the system was cut by a factor of 2-4 when the t/t loop was closed. After considering other possibilities, including loss of light in the border between quad-lenses, we realized that the problem lay in the fact the throughput of the 100 micron, 0.18NA fiber was a function of incidence angle. The throughput plot was a gaussian-shaped curve that fell to approximately 30% of peak at an incidence angle of 0.18 (radians) (see figure 6). Since the light that was on-axis with respect to the t/t sensor was incident on the fiber at an angle of 0.20 radians, the throughput with the loop closed was about 30%, whereas if the light were off-axis on the sensor, the incidence angle of the light on the fiber was smaller, so the throughput was greater. For example, if we started with the light 2 arcsec off-axis, we would have about 80% throughput. After closing the loop, the star is "pulled" towards the center, which increases the light level to the APD until the star is perhaps 1.3 arcsec off-axis. As the star is drawn towards the center of the quad-lens, the throughput of the fiber drops until it reaches about 30% in steady-state closed-loop.

This behavior was not enough to make the behavior of the control loop unstable, but it was enough to reduce the signal to noise ratio of the t/t measurement and reduce the limiting magnitude of usable t/t stars.

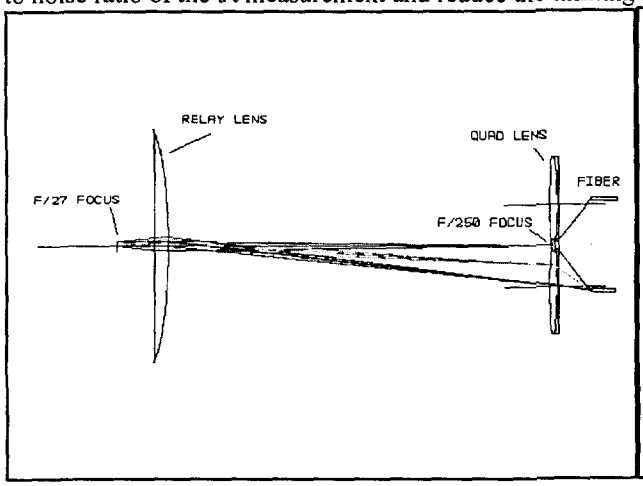

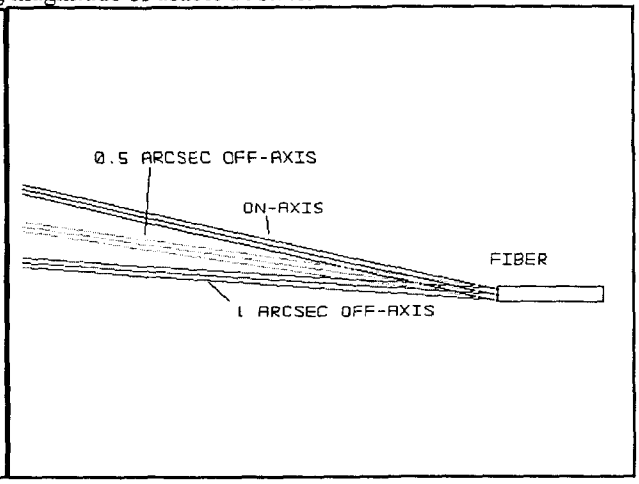

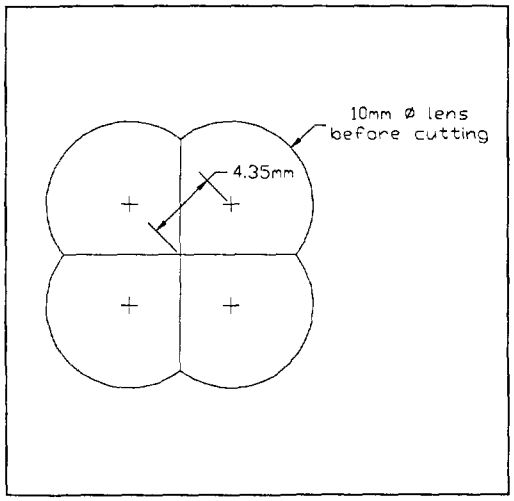

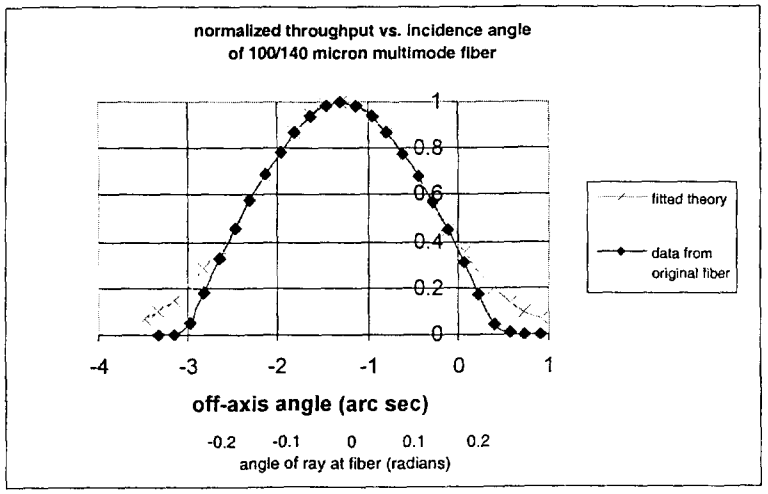

Figure 3 (upper left): Original t/t sensor. Scale is anamorphic.

Figure 4 (upper right): Rear portion of t/t sensor. Note that the on-axis rays strike the fiber face at an angle. Scale is not anamorphic.

Figure 5 (lower left): Quad-lens arrangement for t/t sensor. Optical axes of lenses are indicated with crosses.

Figure 6 (lower right): Throughput of 100/140 micron multimode fiber with nominal NA of 0.18. The bottom horizontal axis indicates the fiber throughput as a function of ray angle. An angle of 0.18 corresponds to the nominal numerical aperture of the fiber. This plot was obtained with a setup that did not include a quad lens so the losses reflect only fiber throughput. The interpretation of angle of ray to off-axis angle was made analytically using parameters from the original t/t sensor design.

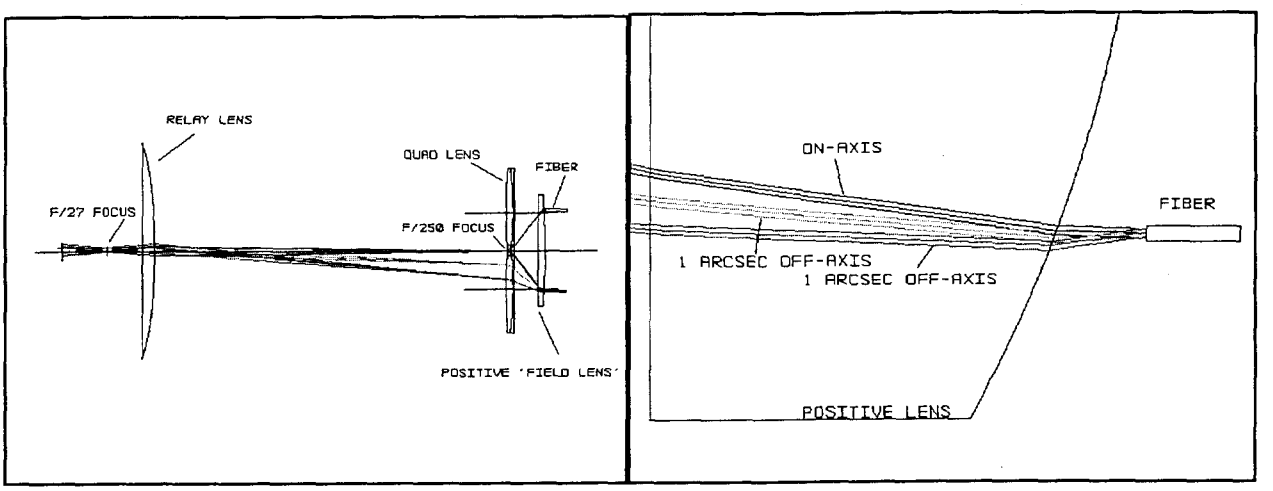

Figures 7 and 8: T/t sensor after adding lens in front of fibers, with magnified view near the fiber. Note that rays from the on-axis field point now strike the fiber face near normal incidence.

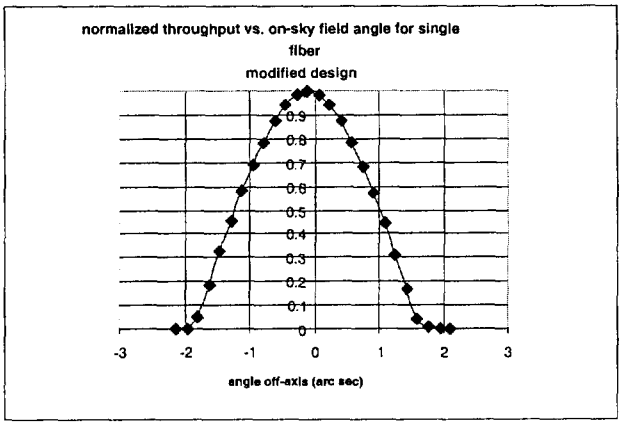

Figure 9: Throughput of t/t sensor after inserting lens before fibers. Note that the peak throughput is near on-axis field angles.

The solution was to change the t/t sensor design so that the on-axis (with respect to the t/t sensor) light was normally-incident to the fiber. One approach might have been to change the mechanical angle at which the fibers were fixed in the t/t sensor. Since that was a fairly expensive change to make, we found another solution: we inserted a lens just before the fibers which steered the light back towards normal incidence, as shown in figures 7 and 8. The focal length of the lens was approximately the distance between the quad lens array and the fiber. This arrangement produces a lower throughput for field angles far from the t/t sensor optical axis, but the on-axis performance (where the tip tilt sensor will operate in closed-loop mode) is excellent (figure 9). It is far more desirable to optimize the system for closed-loop operation than to maximize the capture range for all star magnitudes. With the current design, the capture range is still 2 arcsec in diameter for an m_v=16.25 star.

Of course, the key to proper operation of the t/t sensor is good alignment. Proper positioning of the fiber is more sensitive than one might first think. The FOV of the t/t sensor is ±1 arcsec; with the reduction of the 3m telescope aperture down to 90μ (to fit within a 100μ fiber), the magnification is 3m/90μ=33000! Thus, the ±1 arcsec field is magnified to ±9.3°, which is a slope of ±0.16. As a result, if the fiber face is 1mm away from the correct pupil, then the beam on the fiber will wander by ±0.16*1mm=±160 microns, which is more than the fiber core diameter! We need to position the fiber to an accuracy of about 2% of this number, so we need to set the focus of the fiber to within ~20 microns. This is possible in our setup, but if we wanted to double our tolerance, we could double the FOV to ±2 arcsec at the expense of greater sky background on the t/t sensor. Curiously, while the imaging of the pupil is exacting, the imaging of the t/t star is less so. A 1mm error in focus produces only a marginally larger spot (0.1 arcsec larger) on the quad lens, but has almost no effect on pupil imaging since the exit pupil of the AO system is several meters away.

The size and position of the pupil on the fiber were verified off the AO bench by placing a target that matched the AO system exit pupil location/diameter in front of the t/t sensor, and viewing its image location/size after the t/t sensor with a CCD focused on the fiber face plane. By focusing the camera on a reference mechanical surface and translating in focus by an appropriate, known amount, we could focus the camera on the fiber face plane. By translating the camera and the camera lens on translation stages with precision dial indicators, we could measure the pupil size. Adjustments in pupil size were made by shimming between the quad lens and the final positive lens.

Co-registering the t/t sensor pupil and the AO system pupil is accomplished by back-propagating an incoherent source (e.g., a white light source) through the output end of a t/t fiber and then tracing the light back to the pupil of the system (at the DM plane). Often, this could be conveniently accomplished by evaluating the light pattern a few inches from the cassegrain focus—one could see the "shadow" of the DM pupil mask against the beam from the back-propagating light. Each fiber adjusts a small amount transversely to allow co-alignment of the fiber face and pupil. It is interesting to note that if one fiber is misaligned so that its throughput is low, the control loop will steer the beam so that the diagonally-opposed quadrant has low power as well (by steering the beam away from that quadrant). As a result, two diagonally-opposed quadrants have low power while the other two diagonally-opposed quadrants have high power. With the loop closed, the beam looks as if it is astigmatic, oriented at 45° to the quad lens axes!

2. Calibration method

Calibration of the WFS is important to obtain the highest possible Strehl ratios out of the AO system. Often, people have used a point source (say, a single-mode fiber) at the cassegrain focus position to serve as a reference, and then used image-sharpening techniques or phase-diversity techniques to eliminate the aberrations within the AO bench itself. We have used a somewhat different technique with much success. We have a jig which holds a connectorized single mode fiber at the focus in front of the WFS (see figure 1). This eliminates the off-axis parabolas and 2 other flats as calibration error sources, leaving as the only aberration sources the following: WFS collimating lens, 5 unpowered surfaces, and the internal surfaces of IRCAL. The only powered optic, the collimating lens, is very easy to align to within 100nm P-V error, so the remaining error is just due to non-flatness of the "flats". In any case, we use the same image-sharpening techniques as before to eliminate the residual errors, but the starting point is a much better one with this approach.

The correct position for the jig is determined by propagating an alignment beam forward through the system and maximizing the power through a fiber placed in a fixture at the f/27 focus; the fiber faces the cassegrain focus and is located on an xyz translation stage. Now by propagating coherent light backwards through the fiber at the f/27 focus, we can collimate the fiber position with respect to the second parabola. The position of the fiber is now correct.

3. Rayleigh scattering

In addition to the desired sodium beacon at 90-100km above the earth, the laser produces scattered light in the lower atmosphere, which is appreciable up to about 30km above the earth. In practical LGS operation, an important problem to solve is how to prevent this Rayleigh-scattered light from entering the wavefront sensor. One approach is to launch behind the secondary and use the secondary to block the Rayleigh-scattered light. This can work; the innermost subapertures would see Rayleigh light as close as 2 arcsec off-axis, which can be clipped*. However, limited room between the dome and the secondary require a reflective telescope which is more prone to jitter and misalignment than a refractive telescope.

The side-launching scheme selected for Lick in 1991 has the launch telescope on the south side of the polar-axis-mounted telescope, approximately 2.5 m from the center of the 3m primary. This produces Rayleigh light on the south side of the image plane which needs to be clipped. Table 2 shows the size and off-axis distances of disks of Rayleigh light at various heights in the atmosphere. For this table, the somewhat pessimistic assumption is made that beam size grows linearly from 25cm diameter at the launch telescope to about 1m at 90km; this includes the effects of both uplink

* The baffling offered by the secondary improves considerably with increasing secondary (and presumably telescope) size since the diameter of the launch telescope is fixed at $\sim r_0$ which is telescope-independent.

and downlink seeing.[†] Figures 10 shows the light in the f/27 optical space leading into the WFS; figure 11 is a highly-magnified view of the LGS focal plane in front of the WFS. Note that each scatter point in the atmosphere is imaged by the telescope/AO relay optics to an image in the same f/27 optical space that contains the LGS.

	in object space						in f/27 (WFS) space	
height (km)	off-axis distance (m)	diameter of beam (m)	off-axis distance (urad)	diameter (urad)	off-axis distance (arcsec)	diameter (arcsec)	off-axis distance (mm)	diameter (mm)
10	3.11	0.37	311.1	36.7	64.8	7.6	27.0	3.2
20	2.72	0.43	136.1	21.7	28.4	4.5	11.8	1.9
30	2.33	0.50	77.8	16.7	16.2	3.5	6.8	1.4
40	1.94	0.57	48.6	14.2	10.1	3.0	4.2	1.2
50	1.56	0.63	31.1	12.7	6.5	2.6	2.7	1.1
60	1.17	0.70	19.4	11.7	4.1	2.4	1.7	1.0
70	0.78	0.77	11.1	11.0	2.3	2.3	1.0	1.0
80	0.39	0.83	4.9	10.4	1.0	2.2	0.4	0.9
90	0.00	0.90	0.0	10.0	0.0	2.1	0.0	0.9

Table 2: Size and distance off-axis for sodium guide star beam cross-sections at various heights for telescope at zenith. The launch telescope is 2.5m away from the center of the main telescope with the LGS directly over the main telescope axis; the beam is 25cm at the launch telescope, linearly increasing to 1m at 100km. Heights from 40-80km are included for comparison.

The "traditional approach" to clipping Rayleigh light to use an iris at the sodium guide star image plane to clip out the light that is off-axis. This technique could be used for lasers launched on-axis as well—the iris would then clip out the majority of the out-of-focus Rayleigh-scattered light.

However, this approach turns out to have some important problems which are obvious upon examination.. First, if an iris is used at the sodium guide star image plane, then the Rayleigh light that scatters off the edge of the iris is ***in focus***, i.e., the scattering off the iris edge produces a spurious star which is bright (because the Rayleigh light is very bright) and somewhat off-axis (for a side-launched laser) or forming an annular object around the sodium guide star (for a center-launched laser). In addition, this light will be scattered into all or most of the subapertures—the scatter angle necessary to do this is only ±1° in f/27 space. In either case, the result is problematic since there is generally no other baffling that can prevent this in-focus light from reaching the wavefront sensor. The answer is to clip the Rayleigh light away from the LGS image. It is clear that if the iris edge is brought in from bottom of the diagram, that we will clip Rayleigh light before sodium LGS light. As we continue to bring in the iris edge, if it is located to the left of the LGS image position, then we will clip LGS light before clipping all of the Rayleigh light. If the iris is to the right of the LGS image, then we will clip the Rayleigh completely (or almost completely) before clipping LGS light. Note that the further to the right we place the iris, the more out-of-focus the light scattered off the iris will be; also, the scattered light will affect fewer subapertures and the amount of any clipped LGS light will be smaller. In our setup, the best position is just in front of the next optical surface which is the collimating lens. In figure 11, that would be at the right edge of the figure.

It is worth noting that rejecting Rayleigh light gets more difficult with increase in zenith angle since the Rayleigh light is becoming more distant.

[†] The 25cm diameter waist at the telescope yields a 12.5cm waist radius. The Rayleigh range is w_0^2/λ=(.125m)^2/0.589E-6m=26km.

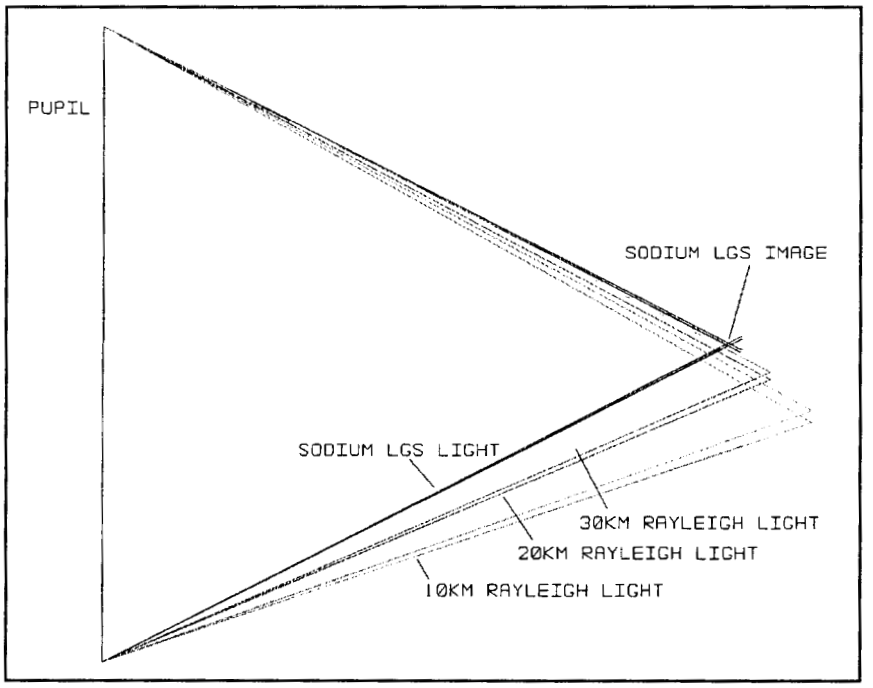

Figure 10 (left): Anamorphic view of sodium LGS light and Rayleigh-scattered light from three lower altitudes in f/27 space. The images of the "disks" of Rayleigh light are at the right edge of the figure.

Figure 11 (below): Close-up of area around f/27 sodium LGS focus, showing proximity of Rayleigh light from different altitudes to the desired sodium beacon light. Note that the scale is anamorphic.

4. Slow wavefront sensor

In LGS mode, the fast WFS is looking at the LGS. Certainly, the distance to the sodium layer changes with zenith angle, and this can be accommodated by moving the WFS stage in focus according to a look-up table. We estimate that in the worst case, the refocusing needs to be done every 4 minutes for 150nm P-V focus error). In addition, though, the sodium layer itself can change in height above the earth, so if the WFS sees a change of focus, we don't know if it is due to a change in telescope/AO bench focus (which we should correct for) or due to a change in the height of the sodium layer (which we should not correct for). In order to tell the difference, we need a "slow" WFS which looks at a natural star. Now, the star to be used for this slow WFS can be the t/t star; this allows us to divert a

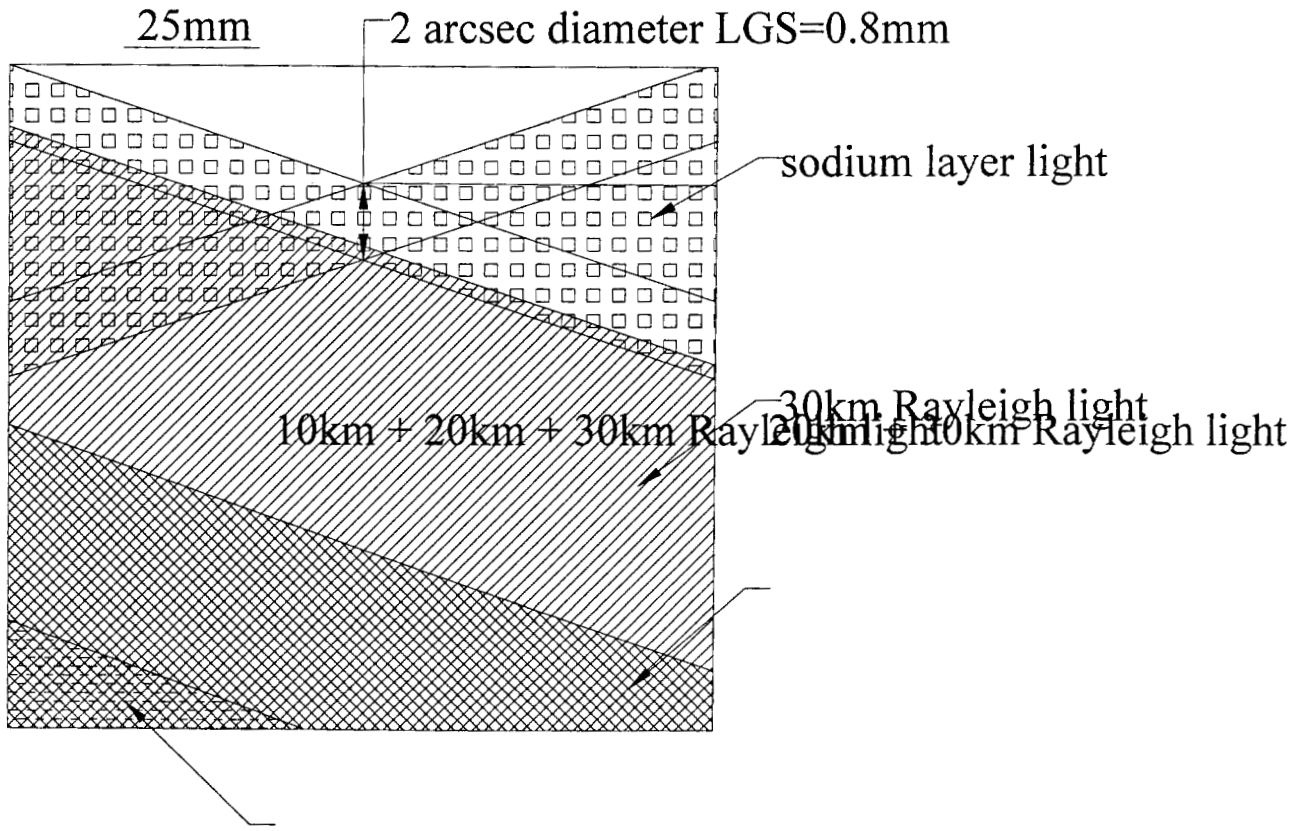

small portion of the light (10%) towards the slow WFS.

Originally, we intended to use a 40 subaperture slow WFS—the same configuration as the fast WFS. The purpose was to be able to calibrate how to change reference centroids when the seeing changed. If WFS's operate with their Hartmann spots on "crosshairs" (centered on the intersection of 4 pixels), then if the seeing (and thus the Hartmann spot size in the poorly-corrected visible spectrum) changed, then there is no effect on where the reference centroids should e. If, however, the centroids are off-crosshairs, then seeing changes would require a change of reference centroids. As our alignment procedures became better defined and our alignments became better, we found that this centroids offsetting as a function of seeing was unnecessary. We decided that it was far better at that point to turn the slow WFS into a focus sensor and to collapse the 40 subapertures into 4, thus increasing the update rate of the sensor by a factor of 10. We now project we can adequately measure the focus mode with an m_V= 17 star with exposures on the order of a minute.

6. FUTURE IMPROVEMENTS

1. Aircraft detection

One nagging operational issue for Lick and for Mauna Kea LGS systems is obtaining spotters to look for airplanes that might come close to entering the beam. Generally, the problem is finding people willing to drive an hour+ to do a not-terribly-interesting job in the middle of a cold night for not much money! At Mauna Kea, we would imagine that these factors become much more difficult!

We are currently working on a design that will use a visible spectrum CCD with a low-distortion, uniform-radiometry fisheye lens to serve as a substitute for these visual observers. The system could be implemented in several ways:

- Mount on top of the dome so as to avoid the parallax problems associated with having a sensor(s) away from the center of the dome. Image comparison would be done to look for rapidly moving objects. This has some problems in that dome rotation is not continuous, but intermittent, so stars will appear to rotate intermittently from frame-to frame in addition to the normal rotation of the sky.
- Mount on non-rotating platform. Again, stars rotate in the field, but for 0.18° pixels (which is the case for 1K pixels across the frame), it takes 40 seconds for a star to transit a pixel. There will be short "streaks" when stars cross pixels. There will be some parallax, but we could ignore the parallax which just treats the laser as if the beam's radius is equal to the distance between the center of the dome and the camera.
- Mount on polar-mounted rotating stage. Stars do not rotate so anything that appears to move is a target of interest. The above comments about parallax apply here also.

Our baseline requirements are as follows:

Requirement	Comment
180°+ field of view (Mauna Kea might require as much as 270°)	Planes have been known to fly near the ground up the neighboring valleys, below the horizon and "suddenly appear" near the dome.
<=1 second for exposure and image comparison	Could be longer at Mauna Kea because there is little to obscure planes; the presence of trees near the Lick dome limits the exposure time.
human-in-loop and semi-autonomous laser shuttering capability	Allows transfer to semi-autonomous operation as experience and confidence in system improves
must "see" planes as well as a human can	For easy-to-understand argument to FAA, who must give approval
Sodium-blocking filter	Avoid saturation by Rayleigh scatter

7. CONCLUSION

The update to the Lick AO bench status has been presented including detailed descriptions of problems and solutions in the areas of t/t sensors, calibration, Rayleigh scatter rejection, and slow wavefront sensors. We have briefly discussed future operational improvements to be made with automated aircraft detection. We believe that Lick Observatory will be soon be able to assume full day-to-day responsibility for the AO system.

8. ACKNOWLEDGMENTS

This work was performed under the auspices of the U.S. Department of Energy by the Lawrence Livermore National Laboratory under contract number W-7405-ENG-48. It was supported by Laboratory Directed Research and Development funding within the University Relations Program and the Lasers Directorate. This support is gratefully acknowledged.

9. REFERENCES

1. Brian J. Bauman, Donald T. Gavel, Gary J. Freeze, Thomas C. Kuklo, Scot S. Olivier, "New optical design of adaptive optics system at Lick Observatory", *Proceedings of the SPIE - The International Society for Optical Engineering, vol. 3760*, (High-Resolution Wavefront Control: Methods, Devices, and Applications, Denver, CO, USA, 19-20 July 1999.), 1999.
2. Claire E. Max, Scot S. Olivier, Herbert W. Friedman, Jong An, Kenneth Avicola, Bart V. Beeman, Horst D. Bissinger, James M. Brase, Gaylen V. Erbert, Donald T. Gavel, Keith Kanz, M.C. Liu, Bruce Macintosh, Kurt P. Neeb, Jennifer Patience, Kenneth E. Waltjen, "Image improvement from a sodium-layer laser guide star adaptive optics system", *Science*, vol.277, pp.1649-52, 1997.
3. S.S. Olivier, C.E. Max, H.W. Friedman, J. An, K. Avicola, B.V. Beeman, H.D. Bissinger, J.M. Brase, G.V. Erbert, D.T. Gavel, IK. Kanz, B. Macintosh, K.P. Neeb, K.E. Waltjen, "First Significant Image Improvement from a Sodium-Layer Laser Guide Star Adaptive Optics System at Lick Observatory", *Proceedings of the SPIE - The International Society for Optical Engineering, vol. 3126*, (Adaptive Optics and Applications, San Diego, CA, USA, 30 July-1 Aug. 1997.), pp.240-8, 1997.
4. Donald T. Gavel, Scot S. Olivier, Brian J. Bauman, Claire E. Max, Bruce A. Macintosh, "Progress with the Lick adaptive optics system", *Proceedings of the SPIE - The International Society for Optical Engineering, vol. 4007,* (SPIE International Symposium on Astronomical Telescopes and Instrumentation 2000, Munich, Germany, March 2000), 2000.
5. Donald T. Gavel, Claire E. Max, Scot S. Olivier, Brian J. Bauman, Deanne M. Pennington, Bruce A. Macintosh, Jennifer Patience, Curtis G. Brown, Pamela. M. Danforth, Randall L. Hurd, Elinor L. Gates, Scott A. Severson, James P. Lloyd, "Science with laser guide stars at Lick Observatory", *Proceedings of the SPIE - The International Society for Optical Engineering, vol. 4494* (SPIE 2001 International Symposium on Optical Science, Engineering, and Instrumentation, San Diego, CA, July 200), 2001.
6. James P. Lloyd, Michael A. Liu, Bruce A. Macintosh, William T. Deich, Scott A. Severson, James Graham, in preparation.
7. Gene Campbell, Brian J. Bauman, Daren Sweider, and Scot S. Olivier, "Adaptive optics system calibration using phase-shifting diffraction interferometer", *Proceedings of the SPIE - The International Society for Optical Engineering, vol. 3760* (SPIE 1999 International Symposium on Optical Science, Engineering, and Instrumentation, Denver, CO, July, 1999), 1999.

This work was performed under the auspices of the U.S. Department of Energy by the University of California, Lawrence Livermore National Laboratory under contract No. W-7405-Eng-48.